ACS Energy LETTERS

http://pubs.acs.org/journal/aelccp

LETTER

Photovoltaic Anodes for Enhanced Thermionic Energy Conversion

A. Bellucci, M. Mastellone, V. Serpente, M. Girolami, S. Kaciulis, A. Mezzi, D. M. Trucchi,* E. Antolín, J. Villa, P. G. Linares, A. Martí, and A. Datas*

Cite This: *ACS Energy Lett.* 2020, 5, 1364−1370

Read Online

ACCESS | Metrics & More | Article Recommendations | Supporting Information

ABSTRACT: Thermionic energy converters are heat engines based on the direct emission of electrons from a hot cathode toward a colder anode. Because the thermionic emission is unavoidably accompanied by photonic emission, radiative energy transfer is a significant source of losses in these devices. In this Letter, we provide the experimental demonstration of a hybrid thermionic−photovoltaic device that is able to produce electricity not only from the electrons but also from the photons that are emitted by the cathode. Thermionic electrons are injected in the valence band of a gallium arsenide semiconducting anode, then pumped to the conduction band by the photovoltaic effect, and finally extracted from the conduction band to produce useful energy before they are reinjected in the cathode. We show that such a hybrid device produces a voltage boost of ∼1 V with respect to a reference thermionic device made of the same materials and operating under the same conditions. This proof of concept paves the way to the development of efficient thermionic and photovoltaic devices for the direct conversion of heat into electricity.

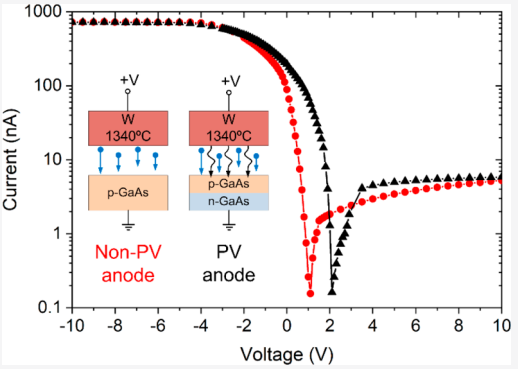

Conversion of heat into electricity is the backbone of all modern economies, generating most of world's electric power. This includes nonrenewable (gas, coal, and nuclear) and renewable (solar thermal and thermal storage) power plants. Virtually all heat engines in operation today are dynamic systems, involving generation of mechanical energy, typically a fluid flow, as an intermediate step for conversion of heat into electricity. These engines are characterized by having a conversion efficiency that increases with the engine size, and this is the reason why current electric systems rely on very large centralized power plants. Contrarily, solid-state alternatives are characterized by having an efficiency that negligibly depends on the device size. This, combined with the lack of moving parts, makes them perfectly suited for electrical power generation at small scales, especially when low maintenance needs are important. This is the case for power generation in space,[1] but also for some other terrestrial applications such as waste heat recovery,[2] combined heat and power (CHP),[3] energy storage,[4−6] or small-scale solar thermal power generators for distributed power generation.[7,8]

Among the solid-state alternatives, thermoelectric generators (TEGs) are the most deployed option.[9] TEG relies on the flow of electrons through a solid, driven by a temperature difference; thus, they are fundamentally limited by the heat conduction losses (phonons flow). These losses preclude the achievement of large temperature gradients and conversion efficiencies, which are typically below 10%.[10,11] Thermionic energy converters (TECs)[12−14] are a high-efficiency alternative to TEGs, where the solid continuity is broken by a nonisothermal vacuum gap that interrupts the phonon propagation, thus avoiding heat conduction losses. The electrons are thermionically emitted from a hot cathode and collected at a cold anode (or collector) to produce an electrical current. TECs have experimentally demonstrated power densities and conversion efficiencies in the range of 10−20 W/cm^2 and 6−13% at cathode temperatures of ∼1530 °C.[15]

There are several sources of losses in TECs that preclude the achievement of higher conversion efficiencies. The most relevant ones are probably related to the thermalization of electrons within the collector and to the voltage losses in the vacuum gap, i.e., the space-charge effect. The former one can be mitigated by using very low work function (ϕ) materials for the anode.[16,17] The latter refers to the accumulation of electrons in the interelectrode vacuum gap, which subsequently creates an electric field that opposes to the electrons' flow. This

Received: January 4, 2020
Accepted: March 24, 2020
Published: March 24, 2020

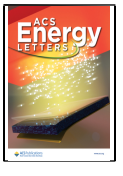

https://dx.doi.org/10.1021/acsenergylett.0c00022
ACS Energy Lett. 2020, 5, 1364−1370

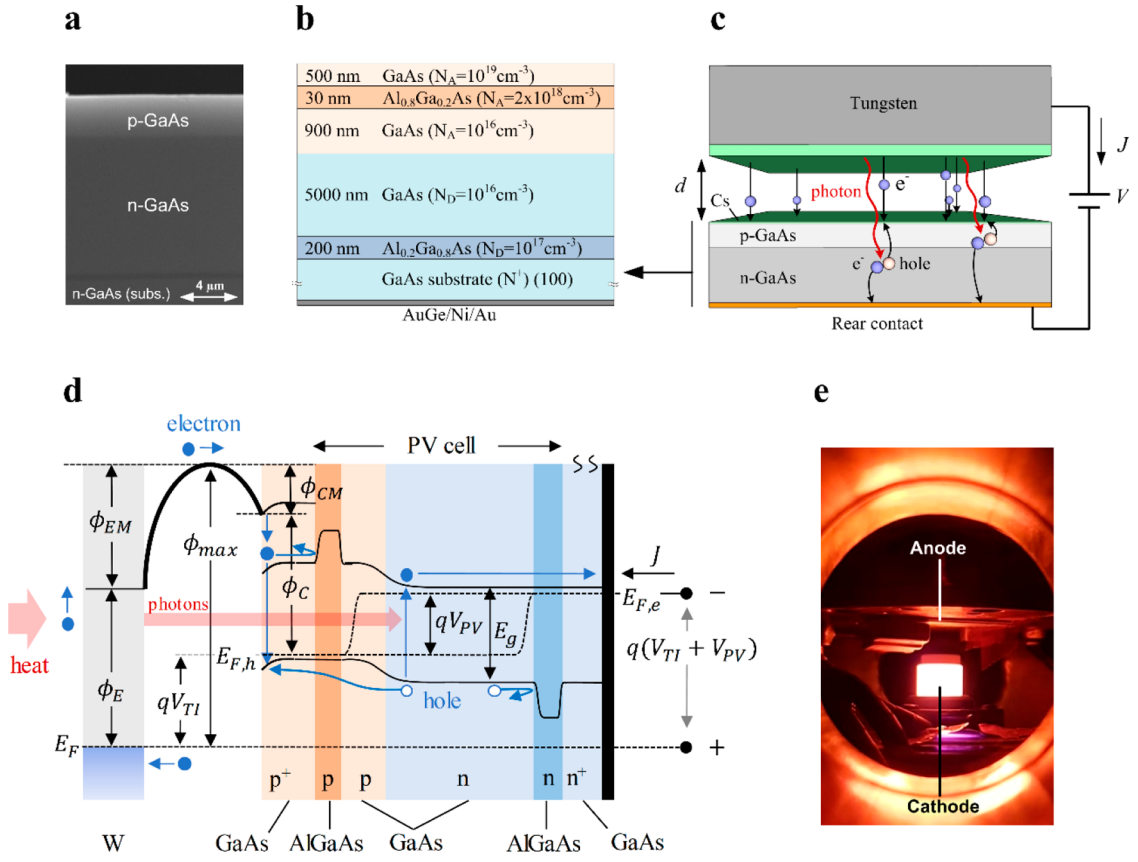

Figure 1. (a) SEM image of the PV cell anode structure; (b) detailed layer structure of the PV cell comprising AlGaAs window and back-surface-field layers and a top highly doped GaAs contact layer; (c) sketch of the complete TIPV converter comprising an emitter (tungsten) and a receiver consisting of a PV cell (GaAs p−n junction) covered by a thin Cs coating; (d) detailed band diagram of the TIPV converter showing the flow of electrons through the device; and (e) picture of the experimental setup in operation at high temperatures, taken from a viewport of the UHV chamber.

effect can be eliminated by reducing the interelectrode distance to micrometric scales.[17−19] However, there exists a minimum distance between the cathode and the anode at which near-field radiative energy transfer significantly contributes to the energy flux and drastically deteriorates the conversion efficiency.[20]

The hybrid thermionic−photovoltaic (TIPV)[21] device has been recently proposed to significantly mitigate the radiative losses and increase the power density of TEC. A TIPV device is a kind of TEC converter in which the anode comprises a photovoltaic (PV) cell that absorbs the radiative flux to produce additional power. The electrons thermionically emitted by the cathode are collected in the anode surface (collector), then injected in the valence band of the PV cell made of a semiconductor with bandgap E_g, and finally pumped to the conduction band upon photon absorption, where they are extracted and delivered to the load (Figure 1c,d). Thus, part of the photon energy (i.e., radiant heat from the cathode) is converted into electrochemical potential (qV_{PV}) within the PV anode (where q is the elementary charge), which is added to that produced by the thermionic stage (qV_{TI}) and results in an enhanced output voltage (V_{PV} + V_{TI}).

Very recently, Schindler et al.[22] observed a TEC voltage boost when illuminating n-GaAs anodes by a 532 nm laser source. The authors argue that this increment in the voltage is attributed to surface photovoltage effect in an n-type semiconductor, which unpins the quasi-Fermi levels at the surface and relaxes the band-bending due to the presence of charged trap states (Figure 2a,b), thus inducing a reduction of the anode work function logarithmically depending on the radiation intensity (up to ∼0.3 eV at 10 mW/cm^2). An alternative explanation could be based on the TIPV mechanisms, though. According to this interpretation, the Fermi level would be still pinned near the mid gap in the n-GaAs anode surface, and thus, the surface work function would be unaltered with respect to the not-illuminated case (Figure 2a,c). The voltage boost would be attributed to the separation of the quasi-Fermi energy levels for the electrons and holes within the semiconductor. Unfortunately, both descriptions are indistinguishable based on the previously reported results, being necessary to hypothesize whether the Fermi energy level is pinned or not at the surface upon illumination.

In this Letter we unequivocally demonstrate a TIPV device in which thermionically emitted electrons are injected in the valence band of a PV cell and subsequently pumped from the valence to the conduction band because of the absorption of photons that are emitted by the cathode (according to the band diagram shown in Figure 1d). We show an enhanced output voltage of ∼1 V with respect to a reference nonphotovoltaic device with identical anode surface termination. This voltage equals the open-circuit voltage independently measured for the PV cell under similar irradiance conditions. Finally, we show that TIPV devices produce a significant enhancement of the electrical power density with

https://dx.doi.org/10.1021/acsenergylett.0c00022
ACS Energy Lett. 2020, 5, 1364−1370

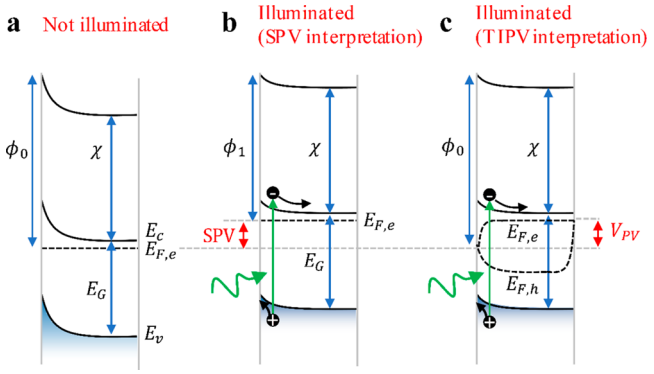

Figure 2. (a) Fermi level pinning in n-type semiconductor creates a Schottky barrier near the surface. (b) Under illumination, and according to the conventional surface photovoltage (SPV) interpretation,[22] holes are injected to the surface creating a dipole that reduces band bending and therefore shifts the Fermi level at the surface toward the vacuum level, ultimately reducing the work function ($\phi_1 < \phi_0$). (c) Under illumination, and according to the TIPV interpretation described in this Letter, the Fermi level remains pinned near the mid gap at the surface, and thus, the work function value is unaltered with respect to the not illuminated case (ϕ_0). The voltage increment takes place within the semiconductor and it originates from the selective extraction of electrons and holes having different quasi-Fermi levels.

respect to the reference thermionic device (~14-fold), especially when using cesium coating in the anode (~240 fold).

In the proposed TIPV device, a p/n GaAs-based PV cell anode structure is used (Figure 1a–d). Although the GaAs PV cell has a too large absorption threshold ($E_G \approx 1.42$ eV), not matching the infrared thermal emission of the cathode, we have chosen this material because of its ability to produce a large open-circuit voltage, which simplifies the experimental validation of the concept, as will be demonstrated below. The PV cell was grown by molecular beam epitaxy (MBE) and comprises a relatively thick (900/5000 nm) GaAs p/n junction sandwiched between two wide-bandgap AlGaAs (~1.85 eV) window layers. These layers are doped with the required polarity to selectively collect the photogenerated electrons (from the rear) and holes (from the front of the device). Their wide bandgap provides the required transparency to allow the photons to be absorbed in the GaAs active layers. A highly doped p-type GaAs contact layer is included in the front to collect the thermionically emitted electrons. This layer brings undesirable absorption losses, but these are tolerable for the aim of this study, which is to experimentally validate the concept. The presence of the p-AlGaAs front window layer guarantees that collected electrons thermalize to the valence band in the topmost p-GaAs contact layer before they are injected into the PV cell (Figure 1d), subsequently ensuring that the Fermi level is pinned near the edge of the valence band at the GaAs/AlGaAs interface. Notice that the Fermi level at the GaAs/vacuum interface is usually pinned near mid gap. This creates a Schottky barrier that ultimately results in a reduction of the work function in a p-GaAs semiconductor under dark conditions (exactly the opposite that for n-GaAs, as shown in Figure 2). If this effect remains under illumination, the maximum TIPV voltage increment (V_{PV}) would be limited to $E_G/2q \approx 0.7$ V. On the other hand, if the Fermi level at the GaAs/vacuum interface surface is unpinned under illumination, the Fermi level could move near the valence band edge; thus, a higher TIPV voltage (approaching $\sim E_G/q$) could be attained. We anticipate that the high voltage enhancements measured in our experiment (~1 V) suggest that the Fermi level at the GaAs/vacuum interface is indeed unpinned, in agreement with the results of Schindler et al.[22] Thus, this is the case illustrated in Figure 1d.

The cathode consists of pure polycrystalline tungsten (W), which is heated by a high-power laser source in ultrahigh vacuum conditions up to temperatures in the range of 1000–1400 °C and moved finely close to the PV cell surface using a micropositioner (Figure 1e). All experiments are conducted at a mean interelectrode distance of 125 ± 20 μm. No significant changes in the I–V curve are observed for such confidence margin, especially regarding the open-circuit voltage (Figure S2 in the Supporting Information). A detailed description of the experimental setup is provided in the Supporting Information (Figure S1). The work function values of (4.6 ± 0.1) eV and (4.5 ± 0.1) eV have been measured for both the PV cell and the cathode surfaces, respectively, by ultraviolet photoelectron spectroscopy (UPS) under dark conditions (Figures S5 and S6). Such high work function values are far from being optimal for thermionic energy conversion and will result in very small current densities and lower output voltages than expected

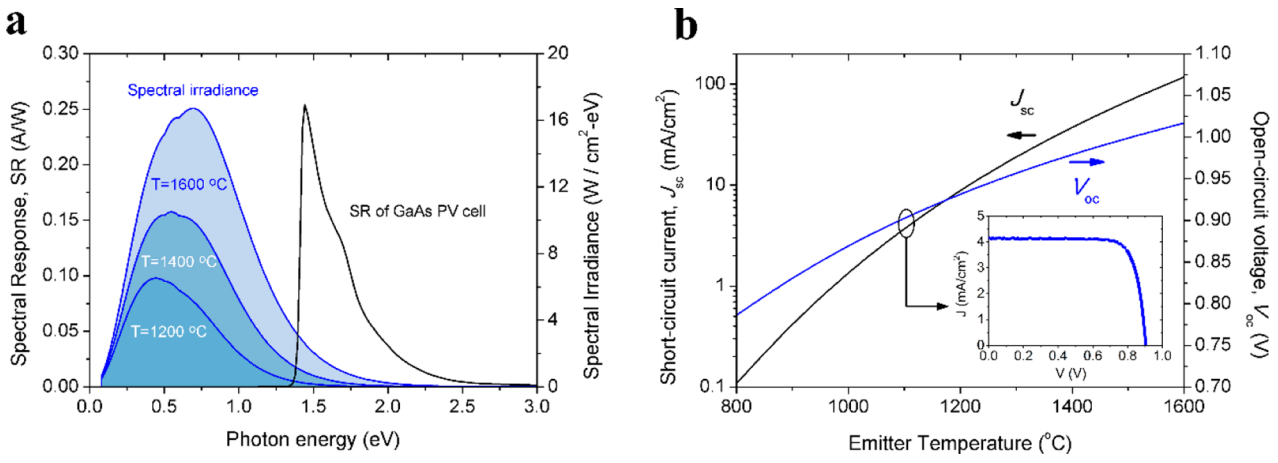

Figure 3. (a) PV cell spectral response and tungsten irradiance and (b) PV cell short-circuit (open-circuit) current (voltage) as a function of the W emitter temperature.

https://dx.doi.org/10.1021/acsenergylett.0c00022
ACS Energy Lett. 2020, 5, 1364–1370

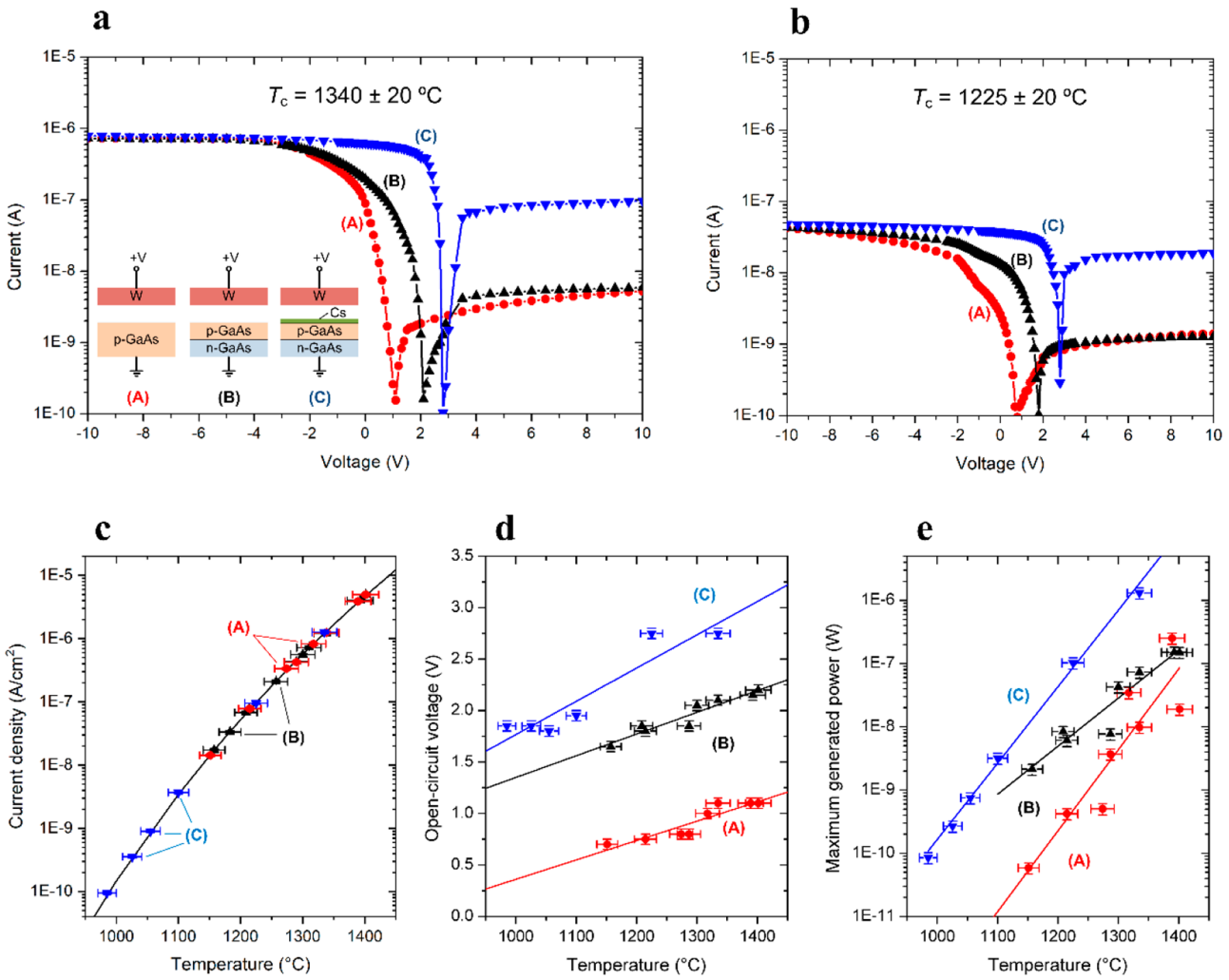

Figure 4. Electric output characteristics of thermionic (A) and TIPV (B and C) converters. The configuration of the three kinds of devices (A, B, and C) is illustrated in the inset of panel a. The thermionic reference device (A) comprises a p-type GaAs anode, while the TIPV devices (C) and (B) comprises a p/n GaAs PV anode structure with and without a thin Cs coating, respectively. The complete *I*−*V* curves are shown for two temperatures: 1340 ± 20 °C (a) and 1225 ± 20 °C (b). Panel c shows the forward saturation current density ($I_{S,F}$) as a function of temperature, along with the corresponding Richardson−Dushman current for ϕ = 4.50 eV and A_R= 60 A cm^{-2} K^{-2}. Panels d and e show the open-circuit voltage and the maximum power generated by the three devices, respectively.

under ideal conditions. Although reducing the work function of the electrodes is mandatory to reach high conversion efficiencies, this is not necessary to demonstrate the operation principles of the concept.

As explained above, thermionically emitted electrons are injected in the valence band of the PV cell, causing holes to drift to the anode surface (Figure 1d). Thus, assuming a negligible recombination of (conduction band) electrons at the GaAs/AlGaAs interface, the rate of thermionically collected electrons and the rate of photogenerated holes reaching such interface must be identical. This balance is ultimately fulfilled by the automatic tuning of the internal voltages V_{PV} and V_{TI}. The maximum rate of photogenerated holes reaching that interface can be calculated through the integration over the whole spectrum of the measured short-circuited PV cell spectral response (in A/W) times the spectral power radiated by the tungsten emitter (in W/cm^2-eV), which is calculated, in this case, by multiplying Planck's law by the tabulated data for tungsten spectral emissivity.[23] Both magnitudes are shown in Figure 3a. The very small overlap between them results in a relatively low short-circuit current density (e.g., 37.8 mA/cm^2 at 1400 °C) but a significant open-circuit voltage (e.g., 0.97 V for a cathode/PV cell temperature of 1400 °C/25 °C), as shown in Figure 3b, which will suffice to validate the concept.

Figure 4 shows the electric output characteristics at different cathode temperatures for three different anode structures: (A) a highly doped p-type GaAs wafer (N_A= 9 × 10^{18} cm^{-3}), (B) a GaAs PV cell with a p/n structure as the one depicted in Figure 1, and (C) the same PV cell structure but incorporating a thin Cs coating (thermally deposited in situ within the characterization chamber from a dispenser). Bias voltage is applied between the cathode (positive terminal) and the anode (negative terminal), as indicated in Figure 1c,d and the inset of Figure 4a. The measured current is the net one resulting from the difference between the forward current, associated with electrons emitted from the cathode to the anode, and the reverse current, associated with electrons emitted back from the anode to the cathode. Negative voltages accelerate the electrons when they travel from the cathode to the anode, resulting in an increment of the current until it reaches a saturated forward value ($I_{S,F}$) at large negative voltages determined by the maximum number of electrons that the

https://dx.doi.org/10.1021/acsenergylett.0c00022
ACS Energy Lett. 2020, 5, 1364−1370

cathode can emit at its hot operation temperature. Equivalently, positive voltages accelerate the electrons when they travel from the anode to the cathode, thus producing a decrement on the current until it reaches a saturated negative reverse value ($I_{S,R}$) at large positive voltages determined by the maximum number of electrons that the anode can emit at its cold operation temperature. The small region in which both the voltage and the current are positive is the power generation quadrant, in which the internal electric field opposes the net electron flow traveling from the cathode to the anode (i.e., retarding region).

Panels a and b of Figure 4 show the current−voltage characteristic (in absolute value) for the three kinds of devices at two different cathode temperatures. The two devices with the same anode surface termination (A and B) provide the same forward and reverse saturation currents ($I_{S,F}$ and $I_{S,R}$, respectively). This implies that both devices can be regarded identical in terms of thermionic properties, as further demonstrated by UPS spectra conducted in dark conditions (Figure S6). In contrast, and as could be expected, the device having a Cs-coated anode surface shows a much higher reverse saturation current, which is induced by its lower work function. Figure 4c shows the forward thermionic saturation current density ($I_{S,F}$), measured at −10 V (interelectrode electric field of $\sim 10^3$ V cm^{-1}), as a function of the cathode temperature for the three kinds of converters (A, B, and C), along with the theoretical Richardson−Dushman current $J_S = A_R T^2 \exp[-\phi/(kT)]$ evaluated for a tungsten cathode under the accelerating regime in a Schottky plot (work function ϕ = 4.50 eV and effective Richardson constant A_R = 60 A cm^{-2} K^{-2}).[12] It is seen that the experimental data fits properly the calculated thermionic current density for the three kinds of devices, implying that the cathodes of the three samples have the same thermionic properties, thus excluding possible contaminations from the anode (e.g., evaporated Cs from anode in sample C).

The relevant main difference observed in all the $I-V$ characteristics is that the hybrid TIPV devices produce larger positive voltages than the corresponding thermionic reference converter for the same cathode temperature and current density. We argue that this higher voltage is attributed to the additional voltage produced by the PV cell (from sample A to sample B). In this regard, notice that the forward saturation current shown in Figure 4c is more than 3 orders of magnitude lower than the maximum photogenerated current in the PV cell (Figure 3b), suggesting that the PV cell is biased near the open-circuit conditions when integrated in the TIPV converter, thus acting as a voltage generator. This hypothesis agrees with the results observed in Figure 4d, which shows the open-circuit voltage V_{oc} of the three devices as a function of the cathode temperature. The difference in open-circuit voltage between GaAs-terminated TIPV (B) and the reference device (A) is ∼1 V for the temperature range of 1100−1400 °C, which equals the open-circuit voltage of the PV cell illuminated under similar irradiance conditions (Figure 3b). Note that open-circuit represents a condition where both forward and reverse currents are identical. Devices with small reverse current, identical cathode and anode surface temperatures, and work function values (such as samples A and B) should also have the same open-circuit voltage, regardless of possibly different space charge conditions. This is because, under such conditions and near open circuit, both forward and reverse currents are very small, well below the critical current density beyond which space-charge is noticeable. Thus, the difference in open-circuit voltages must be explained solely by the effect of the PV-generated voltage. Furthermore, the higher voltage obtained in sample C must be attributed to the lowering of the work function of the PV anode surface by the Cs-coating, which further demonstrates that it is possible to engineer the PV anode surface with low work function materials without suppressing the generation and successive recombination of photogenerated holes with thermionically emitted electrons near the anode/vacuum interface. For sake of completeness, in the Supporting Information we show that the same voltage enhancement of ∼1 V is observed between Cs-coated p/n-GaAs PV and Cs-coated p-GaAs anodes. In addition, we show that a similar work function reduction due to Cs coating is obtained for both p-GaAs and p/n-GaAs anodes in the range of 0.5−0.7 eV.

For the reasons explained above, space-charge conditions do not affect V_{oc}. Conversely, the voltage at the maximum power point V_{op} (namely, the bias voltage maximizing the output electrical power W_{max}), which is typically the main parameter considered for thermionic devices, depends on the presence of space-charge and electron reflection in the anode;[24] therefore, a comparative correlation of V_{op} cannot be taken into account for the concept demonstration. In any case, the corresponding W_{max} is reported in Figure 4e, where the GaAs-terminated TIPV device (B) demonstrates a ∼14-fold power enhancement with respect to the reference thermionic device (A) at 1215 °C. The fact that the output power of the GaAs-terminated TIPV (B) and that of the reference thermionic device (A) converge at high temperatures is probably attributed to the non-well-controlled space-charge and/or electron reflection issues taking place in the vacuum interelectrode gap. The accumulation of charge between the electrodes, which can be accentuated by the presence of electron reflection in the anode,[24] may create an additional barrier when the current increases that precludes the achievement of large thermionic currents at high bias voltages, thus inducing a reduction of the optimum voltage and the maximum output power. Apparently, this effect disappears for the Cs-terminated TIPV device (C), for which an additional 17-fold power enhancement (∼240-fold total power enhancement with respect to the reference device) is observed at the same temperature. This significant power boost can be explained by (1) the higher output voltage attributed to the combined effect of the PV anode and the increased difference in work function between the cathode and the anode and (2) the improved electron collection at the anode, which minimizes electron reflection and the accumulation of charge in the interelectrode gap.

In summary, we have provided experimental evidence indicating that the use of a photovoltaic anode produces a significant increase of the voltage and generated output power with respect to a conventional thermionic energy converter operating under the same conditions. We have also demonstrated the fundamental operational mechanism of hybrid thermionic−photovoltaic energy conversion, i.e., the injection of electrons that are thermionically emitted through vacuum into the valence band of a PV cell that are subsequently pumped to the conduction band upon photon absorption. This represents the implementation of a wireless electric contact on a PV cell, allowing the use of all the surface area and enabling the envisioning of novel device architectures without front metallic grid contacts. For instance, this concept demonstration paves the route to the use of very small interelectrode distances, even approaching the nanometric

https://dx.doi.org/10.1021/acsenergylett.0c00022
ACS Energy Lett. 2020, 5, 1364−1370

scale, at which near-field radiative enhancement and space-charge removal are combined to produce a drastic enhancement of the electrical power density and conversion efficiency.[25−27] This would enable power generation at cathode temperatures much lower than those required by current state-of-the-art TECs, provided that materials with low enough work function are used at both the cathode and the PV cell surfaces. Photon-enhanced thermionic emission (PETE)[28,29] cathodes could be also used for enabling low-temperature near-field TIPV conversion if energy is supplied optically (e.g., concentrated solar power). Optimized near-field TIPV devices have the potential to reach thermal-to-electric conversion efficiencies greater than 30% and power densities beyond 100 W/cm^2 (at 2000 K),[25] outperforming the current state-of-the-art TPV and TEC converters. Thus, future work should focus on developing optimized TIPV converters with smaller and well-controlled interelectrode distances, lower bandgap PV materials, and lower work function coatings for both the electrodes.

■ ASSOCIATED CONTENT

Supporting Information

The Supporting Information is available free of charge at https://pubs.acs.org/doi/10.1021/acsenergylett.0c00022.

Additional data on (i) the methodology for fabricating and characterizing PV cells; (ii) the experimental method used for ultrahigh vacuum and high-temperature thermionic characterization; (iii) sensitivity of the electric $I-V$ characteristics on the interelectrode distance; (iv) the methodology and errors related the cathode temperature measurement; (v) material characterization of anode surface properties, including XRD, AFM, and UPS; and (vi) additional thermionic $I-V$ measurements with cesiated nonphotovoltaic anodes (PDF)

■ AUTHOR INFORMATION

Corresponding Authors

D. M. Trucchi − *Istituto di Struttura della Materia, Consiglio Nazionale delle Ricerche, 00015 Rome, Italy*; Email: danielemaria.trucchi@cnr.it

A. Datas − *Instituto de Energía Solar, Universidad Politécnica de Madrid, 28040 Madrid, Spain*; orcid.org/0000-0001-5964-3818; Email: a.datas@ies.upm.es

Authors

A. Bellucci − *Istituto di Struttura della Materia, Consiglio Nazionale delle Ricerche, 00015 Rome, Italy*; orcid.org/0000-0001-7509-3318

M. Mastellone − *Istituto di Struttura della Materia, Consiglio Nazionale delle Ricerche, 00015 Rome, Italy*

V. Serpente − *Istituto di Struttura della Materia, Consiglio Nazionale delle Ricerche, 00015 Rome, Italy*

M. Girolami − *Istituto di Struttura della Materia, Consiglio Nazionale delle Ricerche, 00015 Rome, Italy*

S. Kaciulis − *Istituto di Studio dei Materiali Nanostrutturati, Consiglio Nazionale delle Ricerche, 00015 Rome, Italy*

A. Mezzi − *Istituto di Studio dei Materiali Nanostrutturati, Consiglio Nazionale delle Ricerche, 00015 Rome, Italy*

E. Antolín − *Instituto de Energía Solar, Universidad Politécnica de Madrid, 28040 Madrid, Spain*; orcid.org/0000-0002-5220-2849

J. Villa − *Instituto de Energía Solar, Universidad Politécnica de Madrid, 28040 Madrid, Spain*

P. G. Linares − *Instituto de Energía Solar, Universidad Politécnica de Madrid, 28040 Madrid, Spain*

A. Martí − *Instituto de Energía Solar, Universidad Politécnica de Madrid, 28040 Madrid, Spain*

Complete contact information is available at: https://pubs.acs.org/10.1021/acsenergylett.0c00022

Author Contributions

A.D. conceived the work; E.A. and A.M. designed and grew the semiconductor structure by MBE; A.D. and P.G.L. fabricated the PV anodes and devices; J.V. performed the PV cell characterization; M.M. and D.M.T. developed and optimized the thermionic−photovoltaic experimental setup; A.B. and D.M.T. coordinated the thermionic−photovoltaic experiments; V.S. performed the Cs deposition; A.B. and M.G. performed the thermionic measurements; S.K. and A.M. performed and analyzed the UPS measurements; A.D., D.M.T., and A.M. analyzed the data and supervised the project. The manuscript was written by A.D. and A.B. with contributions from all authors.

Notes

The authors declare no competing financial interest.

■ ACKNOWLEDGMENTS

This work has been funded by project AMADEUS, which has received funds from the European Union Horizon 2020 research and innovation program, FET-OPEN action, under Grant Agreement 737054. The sole responsibility for the content of this publication lies with the authors. It does not necessarily reflect the opinion of the European Union. Neither the REA nor the European Commission are responsible for any use that may be made of the information contained therein. E.A. acknowledges a Ramón y Cajal Fellowship (RYC-2015-18539) funded by the Spanish Science, Innovation and Universities Ministry. A Young Researcher Grant from Universidad Politécnica de Madrid is acknowledged by E.A. and P.G.L. The authors are also grateful to the reviewers for their valuable suggestions and careful reading.

■ REFERENCES

(1) Datas, A.; Martí, A. Thermophotovoltaic energy in space applications: Review and future potential. *Sol. Energy Mater. Sol. Cells* **2017**, *161*, 285−296.

(2) Orr, B.; Akbarzadeh, A.; Mochizuki, M.; Singh, R. A review of car waste heat recovery systems utilising thermoelectric generators and heat pipes. *Appl. Therm. Eng.* **2016**, *101*, 490−495.

(3) Qiu, K.; Hayden, A. C. S. Integrated thermoelectric and organic Rankine cycles for micro-CHP systems. *Appl. Energy* **2012**, *97*, 667−672.

(4) Datas, A.; Ramos, A.; del Cañizo, C. Techno-economic analysis of solar PV power-to-heat-to-power storage and trigeneration in the residential sector. *Appl. Energy* **2019**, *256*, 113935.

(5) Datas, A.; Ramos, A.; Martí, A.; del Cañizo, C.; Luque, A. Ultra high temperature latent heat energy storage and thermophotovoltaic energy conversion. *Energy* **2016**, *107*, 542−549.

(6) Amy, C.; Seyf, H. R.; Steiner, M. A.; Friedman, D. J.; Henry, A. Thermal energy grid storage using multi-junction photovoltaics. *Energy Environ. Sci.* **2019**, *12*, 334−343.

(7) Kraemer, D.; et al. High-performance flat-panel solar thermoelectric generators with high thermal concentration. *Nat. Mater.* **2011**, *10*, 532.

(8) Trucchi, D. M.; et al. Solar Thermionic-Thermoelectric Generator (ST2G): Concept, Materials Engineering, and Prototype Demonstration. *Adv. Energy Mater.* **2018**, *8*, 1802310.
(9) Rowe, D. M. *Thermoelectrics Handbook: Macro to Nano*; CRC Press: New York, 2005.
(10) He, J.; Tritt, T. M. Advances in thermoelectric materials research: Looking back and moving forward. *Science* **2017**, *357*, No. eaak9997.
(11) Liu, W.; Jie, Q.; Kim, H. S.; Ren, Z. Current progress and future challenges in thermoelectric power generation: From materials to devices. *Acta Mater.* **2015**, *87*, 357−376.
(12) Hatsopoulos, G. N.; Gyftopoulos, E. P. *Thermionic Energy Conversion*; The MIT Press: Cambridge MA, 1979; Vol. *I*, Chapter 3.
(13) Abdul Khalid, K. A.; Leong, T. J.; Mohamed, K. Review on Thermionic Energy Converters. *IEEE Trans. Electron Devices* **2016**, *63*, 2231−2241.
(14) Go, D. B.; et al. Thermionic Energy Conversion in the Twenty-first Century: Advances and Opportunities for Space and Terrestrial Applications. *Front. Mech. Eng.* **2017**, *3*, 13.
(15) Becker, R. A. Thermionic space power systems review. *J. Spacecr. Rockets* **1967**, *4*, 847−851.
(16) Kim, S.; Lee, M. Y.; Lee, S.; Jhi, S.-H. Super low work function of alkali-metal-adsorbed transition metal dichalcogenides. *J. Phys.: Condens. Matter* **2017**, *29*, 315702.
(17) Yuan, H.; et al. Back-gated graphene anode for more efficient thermionic energy converters. *Nano Energy* **2017**, *32*, 67−72.
(18) Belbachir, R. Y.; An, Z.; Ono, T. Thermal investigation of a micro-gap thermionic power generator. *J. Micromech. Microeng.* **2014**, *24*, 085009.
(19) Lee, J. H.; et al. Microfabricated Thermally Isolated Low Work-Function Emitter. *J. Microelectromech. Syst.* **2014**, *23*, 1182−1187.
(20) Lee, J.-H.; Bargatin, I.; Melosh, N. A.; Howe, R. T. Optimal emitter-collector gap for thermionic energy converters. *Appl. Phys. Lett.* **2012**, *100*, 173904.
(21) Datas, A. Hybrid thermionic-photovoltaic converter. *Appl. Phys. Lett.* **2016**, *108*, 143503.
(22) Schindler, P.; et al. Surface Photovoltage-Induced Ultralow Work Function Material for Thermionic Energy Converters. *ACS Energy Lett.* **2019**, *4*, 2436−2443.
(23) Siegel, R.; Howell, J. R. *Thermal Radiation Heat Transfer*; McGraw Hill: New York, 1972.
(24) Lim, I. T.; Lambert, S. A.; Vay, J.-L.; Schwede, J. W. Electron reflection in thermionic energy converters. *Appl. Phys. Lett.* **2018**, *112*, 073906.
(25) Datas, A.; Vaillon, R. Thermionic-enhanced near-field thermophotovoltaics. *Nano Energy* **2019**, *61*, 10−17.
(26) Datas, A.; Vaillon, R. Thermionic-enhanced near-field thermophotovoltaics for medium-grade heat sources. *Appl. Phys. Lett.* **2019**, *114*, 133501.
(27) Liao, T.; Zhang, X.; Chen, X.; Chen, J. Near-field thermionic-thermophotovoltaic energy converters. *J. Appl. Phys.* **2019**, *125*, 203103.
(28) Schwede, J. W.; et al. Photon-enhanced thermionic emission for solar concentrator systems. *Nat. Mater.* **2010**, *9*, 762.
(29) Schwede, J. W.; et al. Photon-enhanced thermionic emission from heterostructures with low interface recombination. *Nat. Commun.* **2013**, *4*, 1576.

https://dx.doi.org/10.1021/acsenergylett.0c00022
ACS Energy Lett. 2020, 5, 1364−1370